Supplementary Material for

Understanding Supercapacitive Performance of N-doped Vanadium Carbide/Carbon Composite as Anode Material in an All Pseudocapacitive Asymmetric Cell

Hem Kanwar Rathore,[1,$] Muruganandham Hariram,[1,$] Mukhesh K Ganesha,[2] Ashutosh K Singh,[2] Debanjan Das,[3] Manoj Kumar,[1] Kamlendra Awasthi,[1] Debasish Sarkar[1,*]

[1]Department of Physics, Malaviya National Institute of Technology Jaipur, Rajasthan-302017, India.

[2]Centre for Nano and Soft Matter Sciences, Bengaluru- 562162, India.

[3]Analytical Chemistry and Center for Electrochemical Sciences, Ruhr-University Bochum, 44780 Bochum, Germany

***Corresponding author:** E-Mail: deb.sarkar1985@gmail.com ; debasish.phy@mnit.ac.in

[$]Authors contributed equally to this work.

Electrochemical Performance evaluation of single electrode and asymmetric supercapacitor (ASC)

The gravimetric capacitance (C_s, F/g) and areal capacitance (C_a, F/cm^2) values of the single electrode are estimated from the discharge time of charge-discharge profiles according to the following equations:

$$C_s = \frac{i * \Delta t}{m * \Delta V} \tag{1}$$

$$C_a = \frac{m}{A} C_s \tag{2}$$

where i (A) represents discharge current, Δt (s) is the discharge time, m (g) is the active mass of electrode material, ΔV (V) is the stable potential window, and A (cm^2) refers to the effective surface area of the electrode.

Moreover, capacitance values are also estimated from the area under cyclic voltammograms (CV) at a specific scan rate according to the following equations:

$$C_s = \frac{\int i dV}{2 * m * v * \Delta V} \tag{3}$$

$$C_a = \frac{m}{A} C_s \tag{4}$$

where i (A) is the current response, dV (V) is the voltage differential, m (g) is the active mass of material, v (V/s) is the scan rate, and ΔV (V) is the stable operating potential window, and A (cm^2) is the effective surface area of the electrode. The capacitance values of the ASC are estimated from the same equations. However, mass (m, g) in the case of the two-electrode configuration is the total mass of both electrode active materials.

The energy density ($E, Wh/kg$), power density ($P, W/kg$), equivalent series resistance (ESR), and maximum power (P_{max}) of assembled asymmetric supercapacitor (ASC) were measured using these equations:

$$E = \frac{1}{2 * 3.6} C_s \Delta V^2 \tag{5}$$

$$P = \frac{3600 * E}{\Delta t} \tag{6}$$

$$ESR = \frac{iR_{drop}}{2i} \quad (7)$$

$$P_{max} = \frac{\Delta V^2}{4 * ESR * m} \quad (8)$$

where C_s (F/g) is the gravimetric capacitance of the ASC, ΔV (V) is the discharge voltage, Δt (s) is the discharge time, i (A) is the discharge current, and m is the total mass of both electro-active materials.

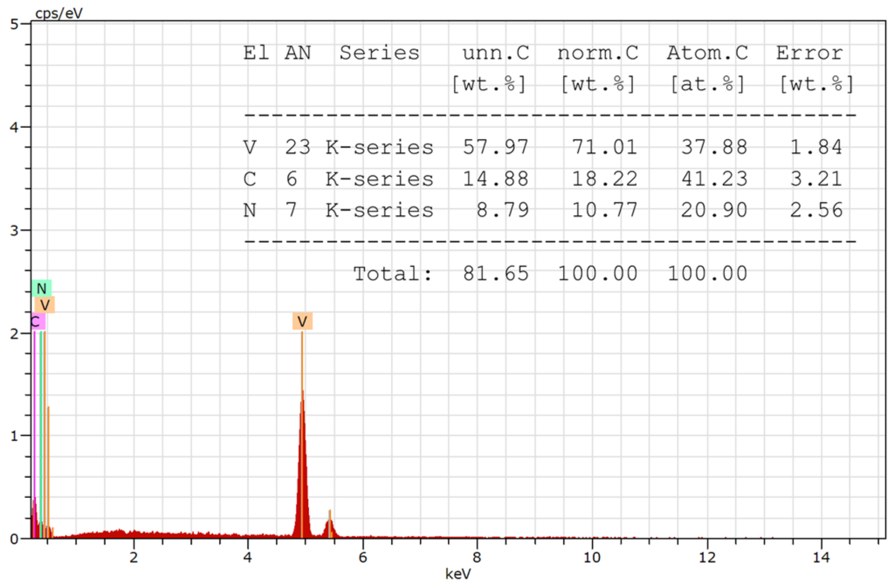

Fig. S1 EDS spectra for as-synthesized N-doped V_4C_3/C nanohybrid.

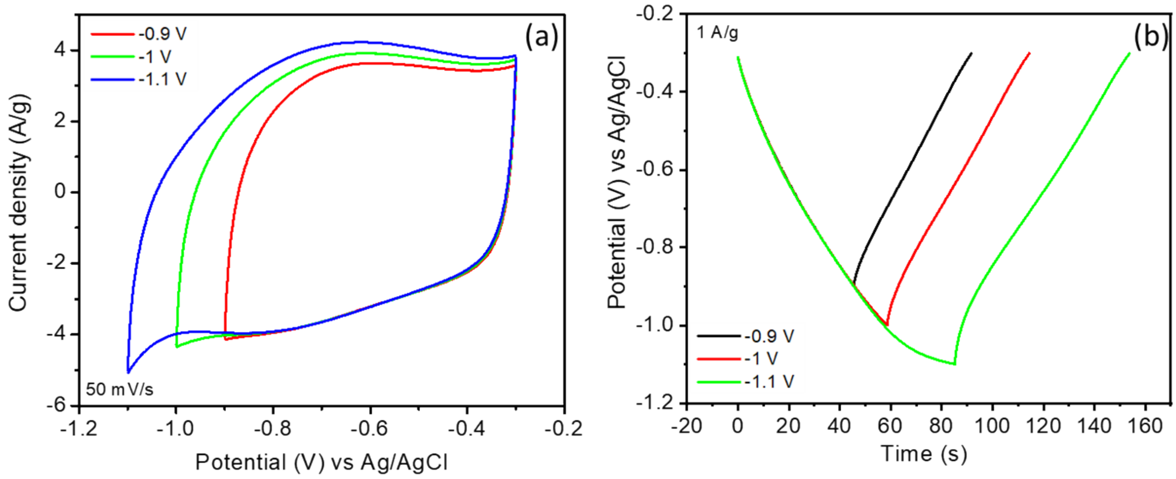

Fig. S2 (a) CV curves, and (b) GCD profiles of N-doped V_4C_3/C nanohybrid in different potential windows.

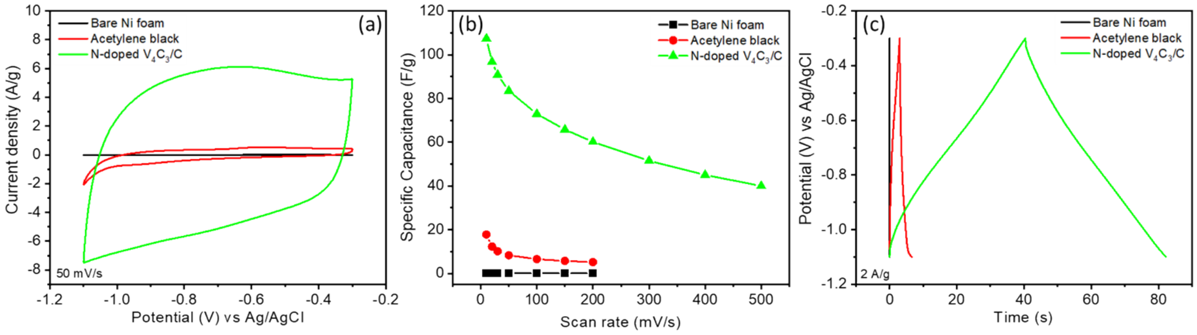

Fig. S3 (a) Comparative CV curves at 50 mV/s scan rate, (b) specific capacitance as a function of scan rate, and (c) GCD profiles at 2 A/g current density of bare Ni foam, acetylene black, and N-doped V_4C_3/C nanohybrid in -0.3 to -1.1 V (vs Ag/AgCl) potential window.

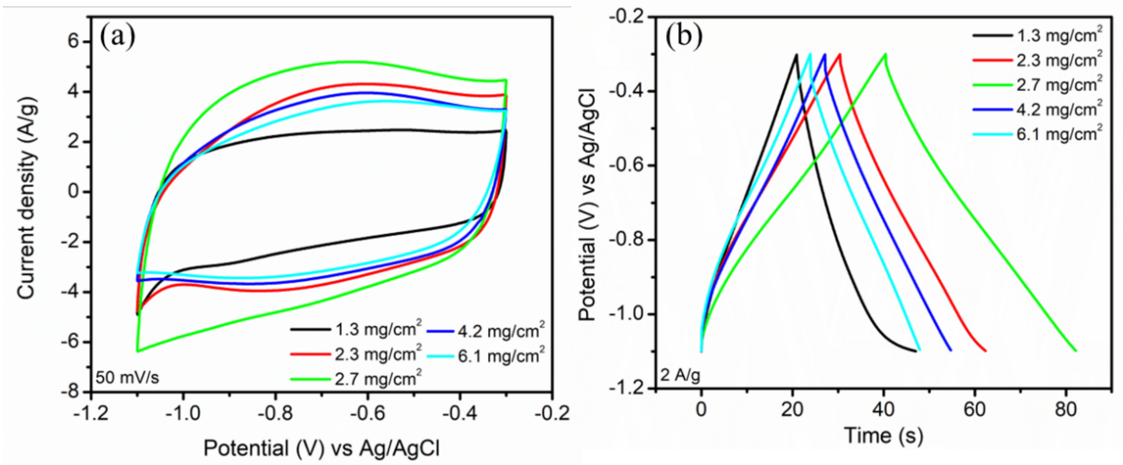

Fig. S4 (a) CV curves of N-doped V_4C_3/C electrodes of different loading densities at 50 mV/s scan rate, and (b) GCD curves of N-doped V_4C_3/C electrodes of different loading densities at 2 A/g current density.

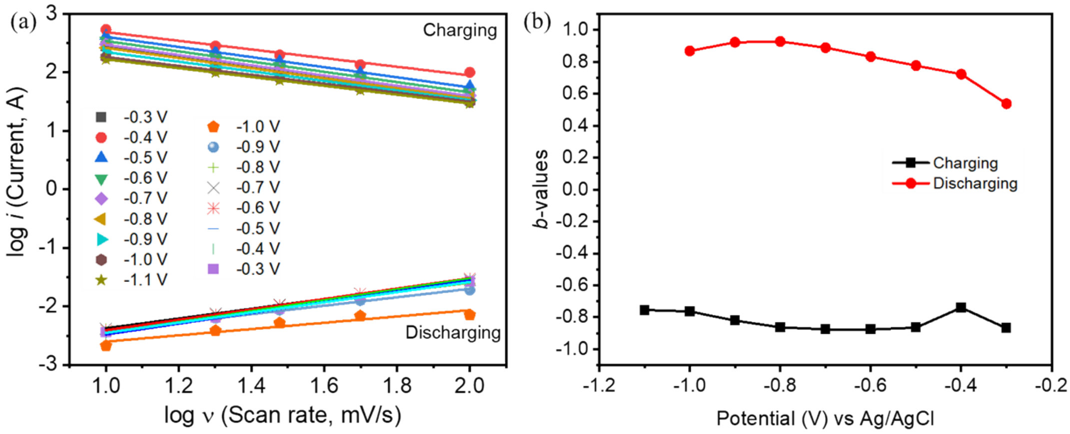

Fig. S5 (a) log *i* versus log *v* plot for charging and discharging of N-doped V_4C_3/C electrode at different voltages, and (b) variation of *b*-values (slope) at different potentials for charging and discharging sweeps of CV.

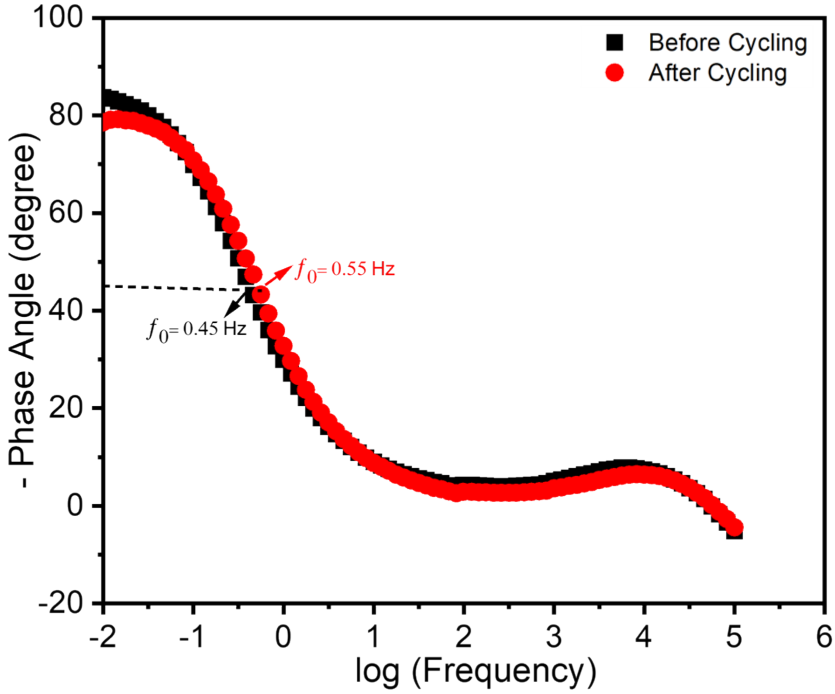

Fig. S6 The Bode plot of N-doped V_4C_3/C electrode before and after cycling tests.

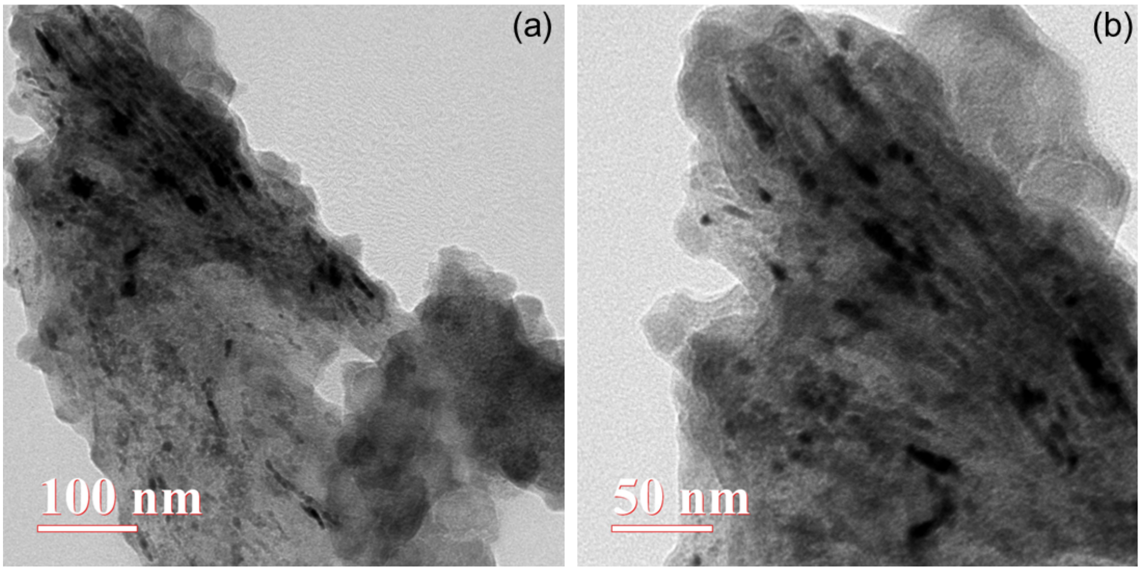

Fig. S7 (a,b) TEM images at different magnifications of N-doped V_4C_3/C after 10,000 CV cycles at 100 mV/s scan rate in half-cell configuration.

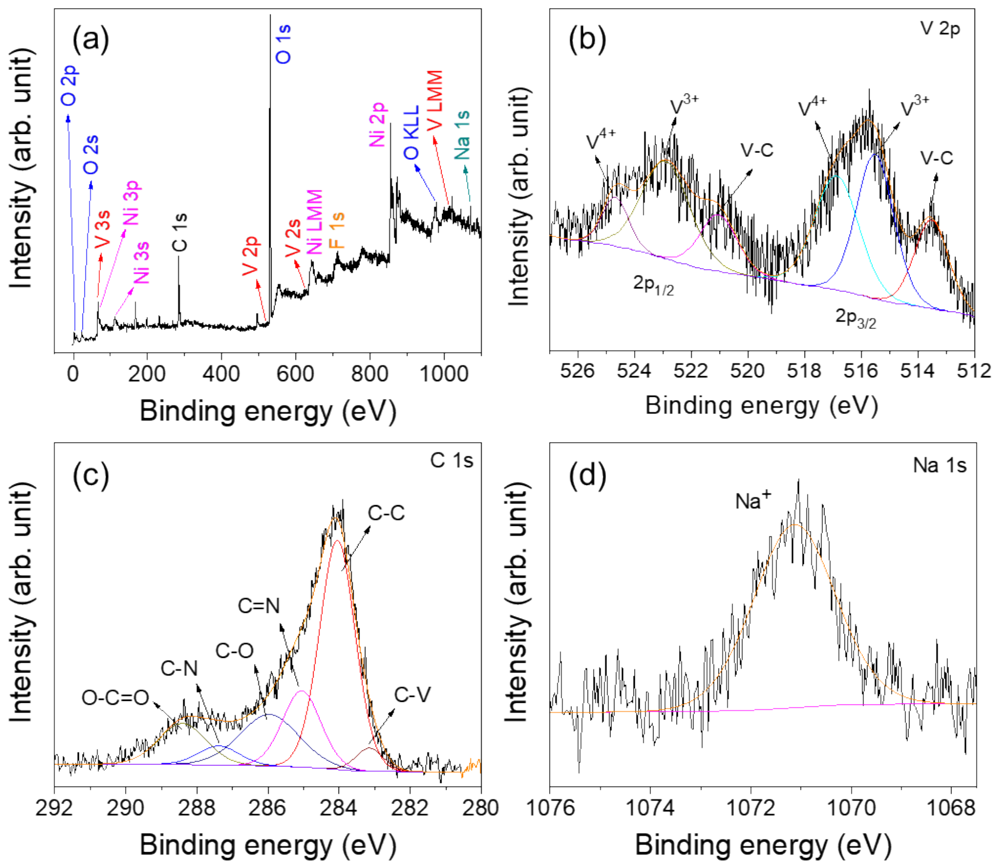

Fig. S8 (a) XPS survey spectra, and high resolution spectra of (b) V 2*p*, (c) C 1*s*, and (d) Na 1*s* of N-doped V_4C_3/C after 10,000 CV cycles at 100 mV/s scan rate in half-cell configuration.

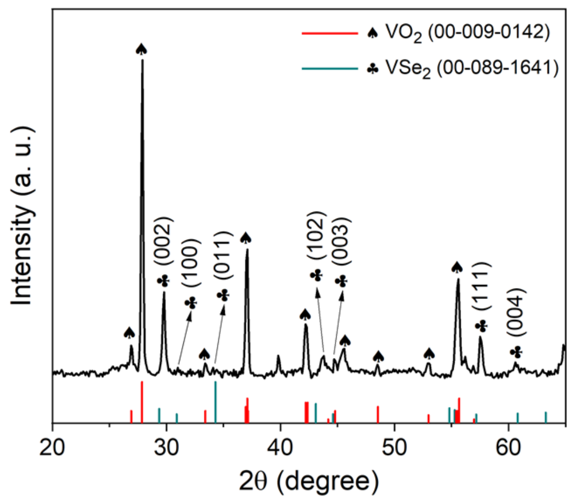

Fig. S9 XRD spectra of as-synthesized VO_2/VSe_2 hybrid nanoflowers. The XRD peaks are indexed with the Bragg reflections of monoclinic VO_2 (JCPDS No.: 09-0142) and hexagonal VSe_2 (JCPDS No. 89-1641).

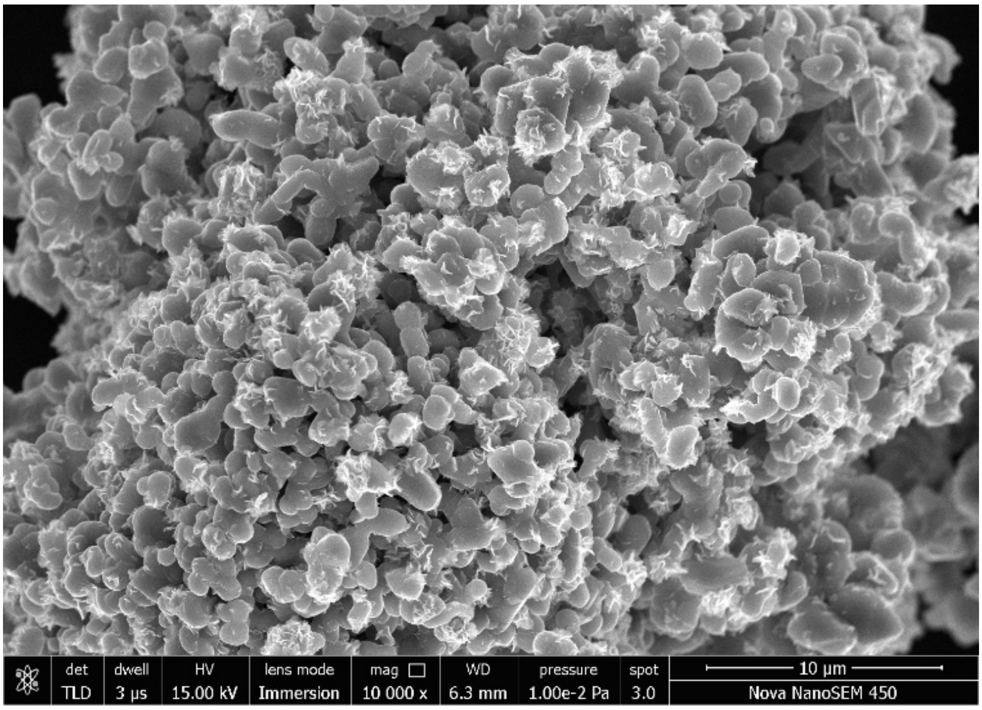

Fig. S10 FESEM image of as-synthesized VO_2/VSe_2 hybrid nanoflowers.

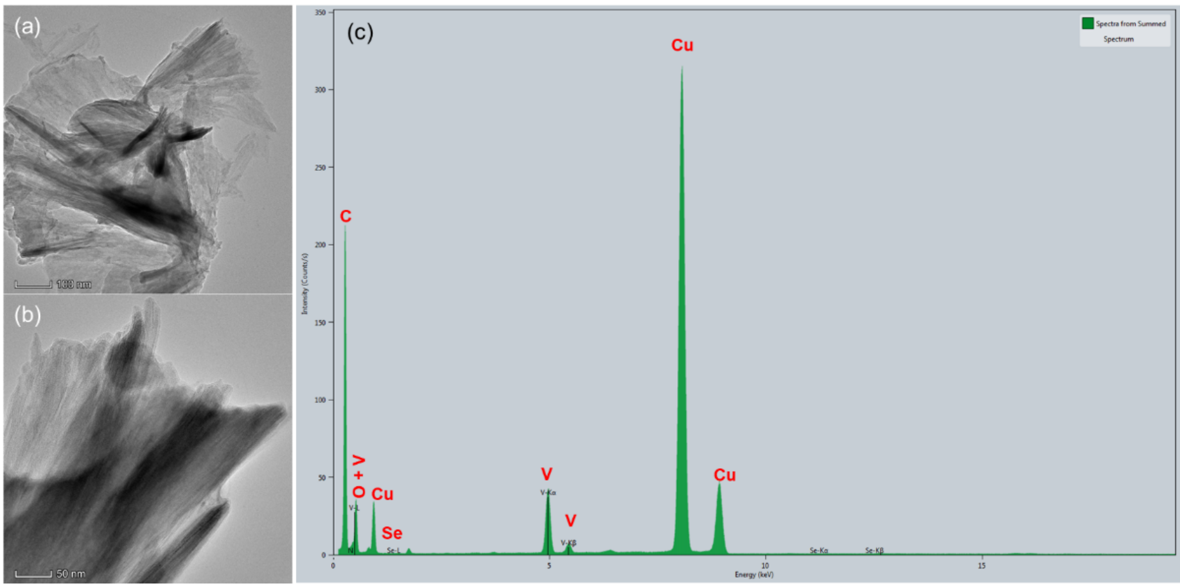

Fig. S11 (a, b) TEM images of VO_2/VSe_2 hybrid nanoflowers, and (c) EDS spectra showing presence of different constituent elements.

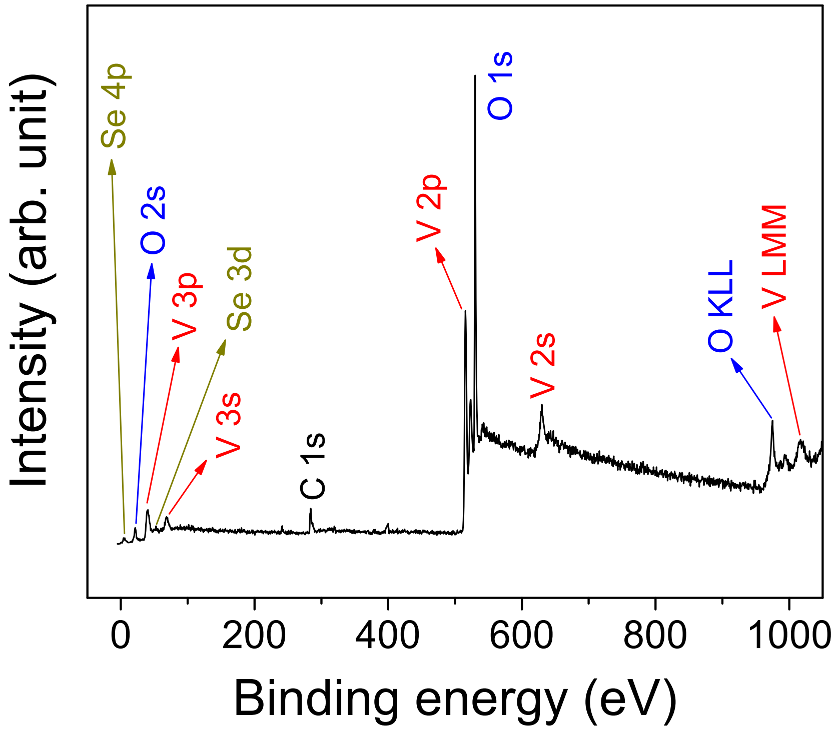

Fig. S12 XPS survey spectra of VO_2/VSe_2 hybrid nanostructures. A minute signal of C could be ascribed to some adventitious C present in the sample.

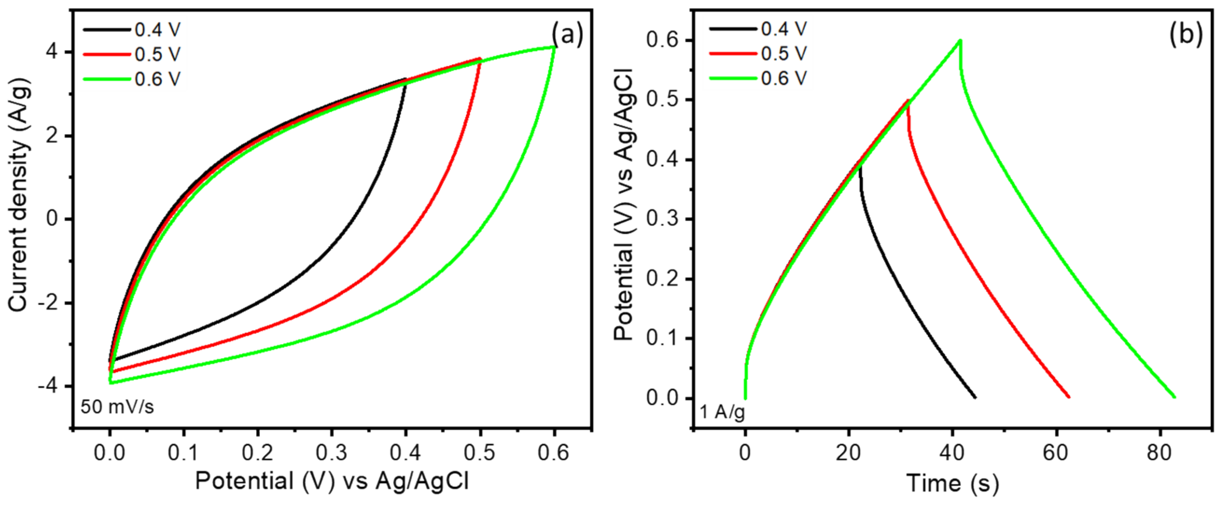

Fig. S13 (a) CV curves at 50 mV/s, and (b) GCD curves at 1 A/g current density of VO_2/VSe_2 electrode at various voltage windows.

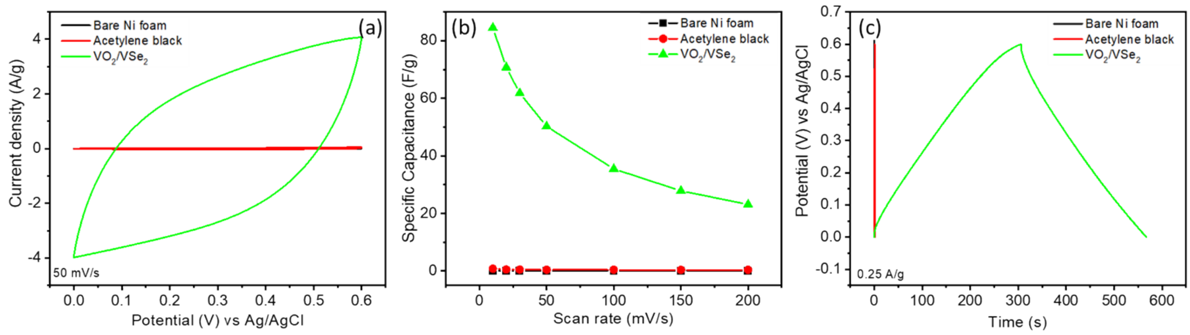

Fig. S14 (a) Comparison of CV curves at 50 mV/s, (b) variation of capacitance with scan rate, and (c) GCD curves at 0.25 A/g current density of bare Ni foam, acetylene black, and VO_2/VSe_2 electrode within 0-0.6 V (vs Ag/AgCl) voltage window.

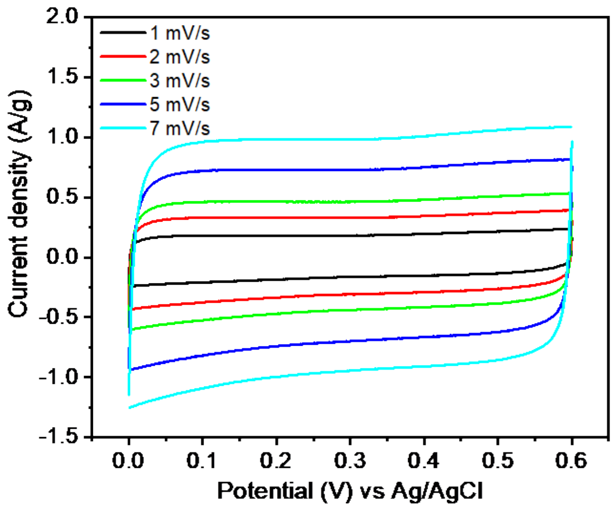

Fig. S15 CV curves of the VO_2/VSe_2 electrode at low scan rates ranging from 1-7 mV/s.

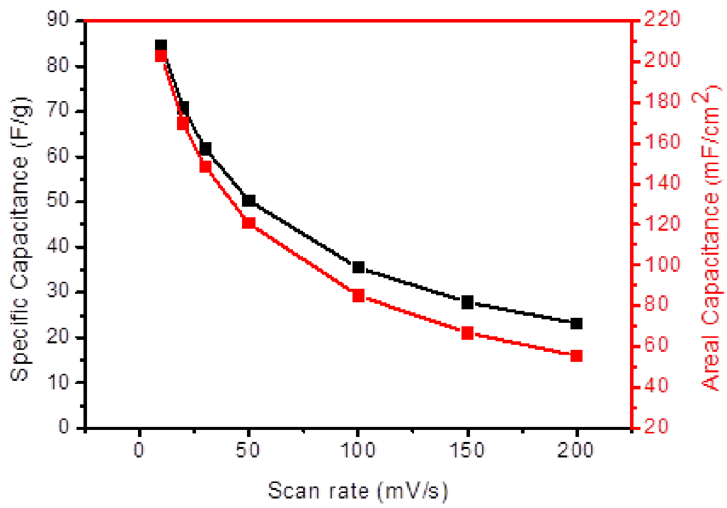

Fig. S16 Variation of capacitance with scan rate for VO_2/VSe_2 hybrid nanostructures.

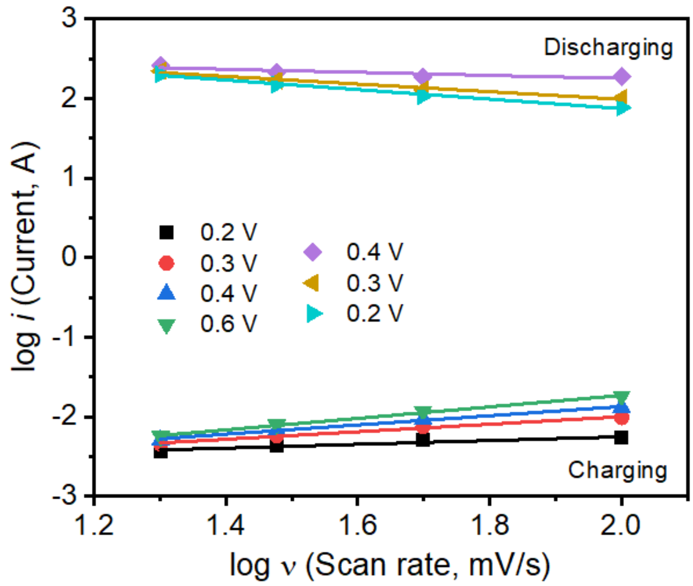

Fig. S17 log *i* versus log *v* plot for charging and discharging of VO_2/VSe_2 electrode at different voltages.

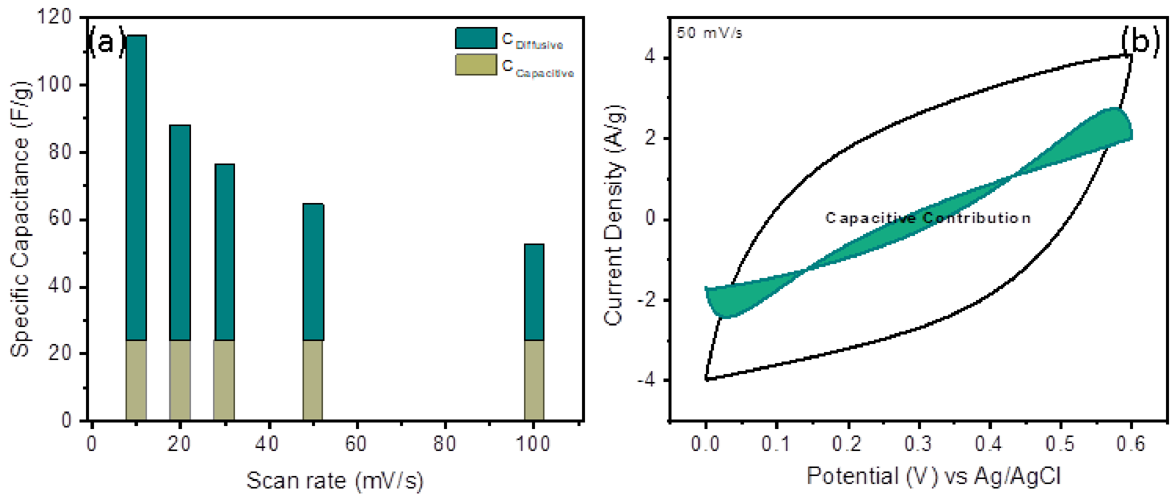

Fig. S18 (a) Contributions from capacitive and diffusive processes of VO_2/VSe_2 electrode at different scan rates, (b) comparison of capacitive (shaded region) and diffusion-dominated charge storage process at 50 mV/s scan rate for VO_2/VSe_2 electrode.

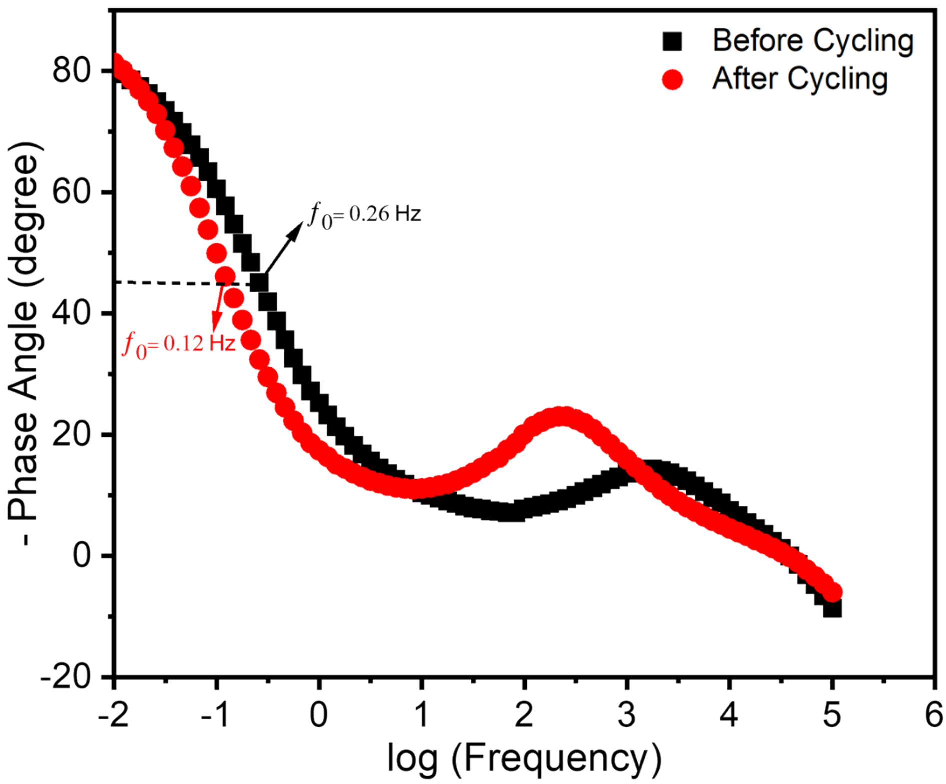

Fig. S19 The Bode plot of VO_2/VSe_2 electrode prior and after cycling test.

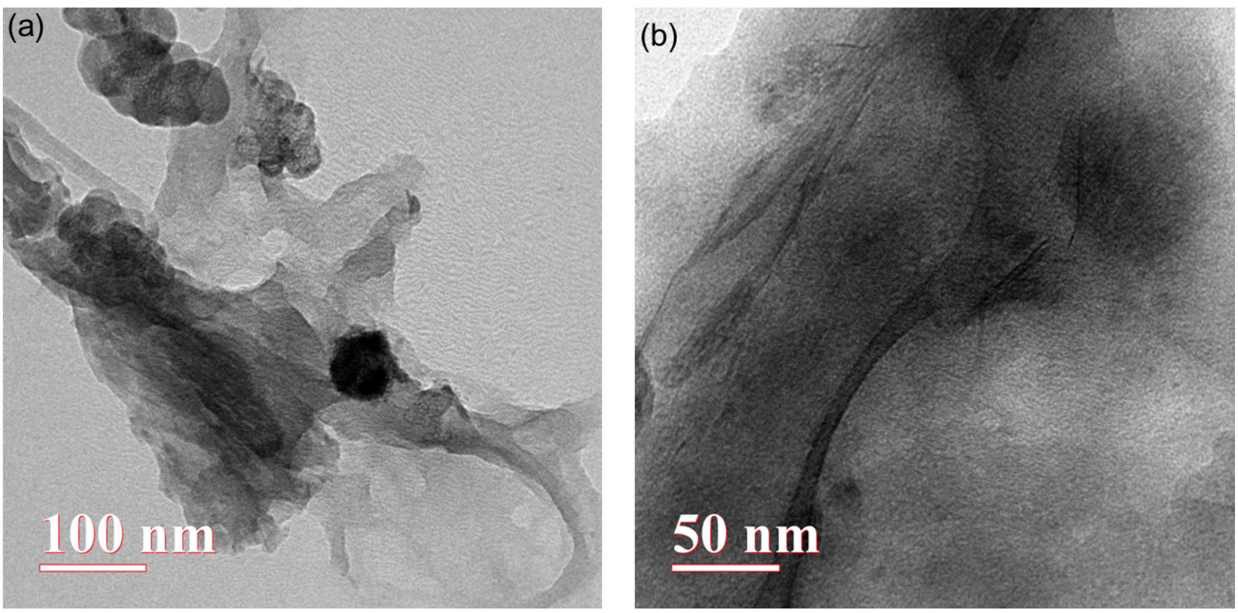

Fig. S20 (a,b) TEM images of VO_2/VSe_2 nanoflower after 10000 CV cycles at 100 mV/s scan rate in half-cell configuration.

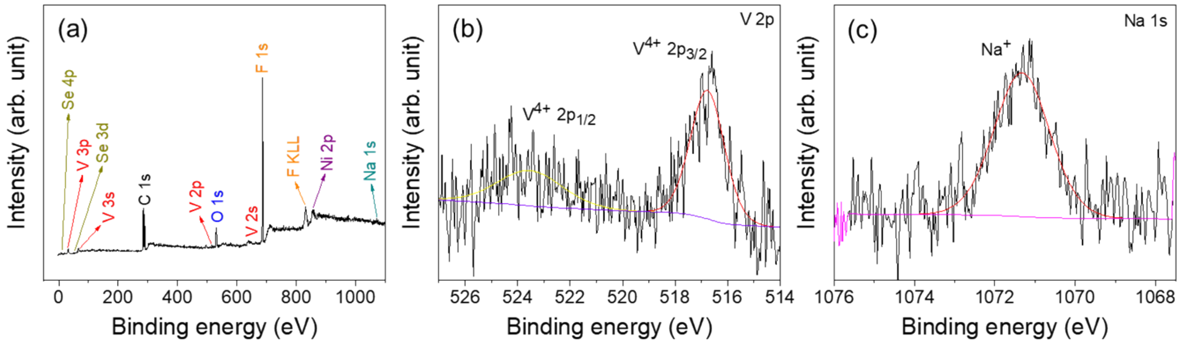

Fig. S21 (a) XPS survey spectra, and high resolution spectra of (b) V 2*p*, and (c) Na 1*s* of VO_2/VSe_2 nanoflower after 10,000 CV cycles at 100 mV/s scan rate in half-cell configuration.

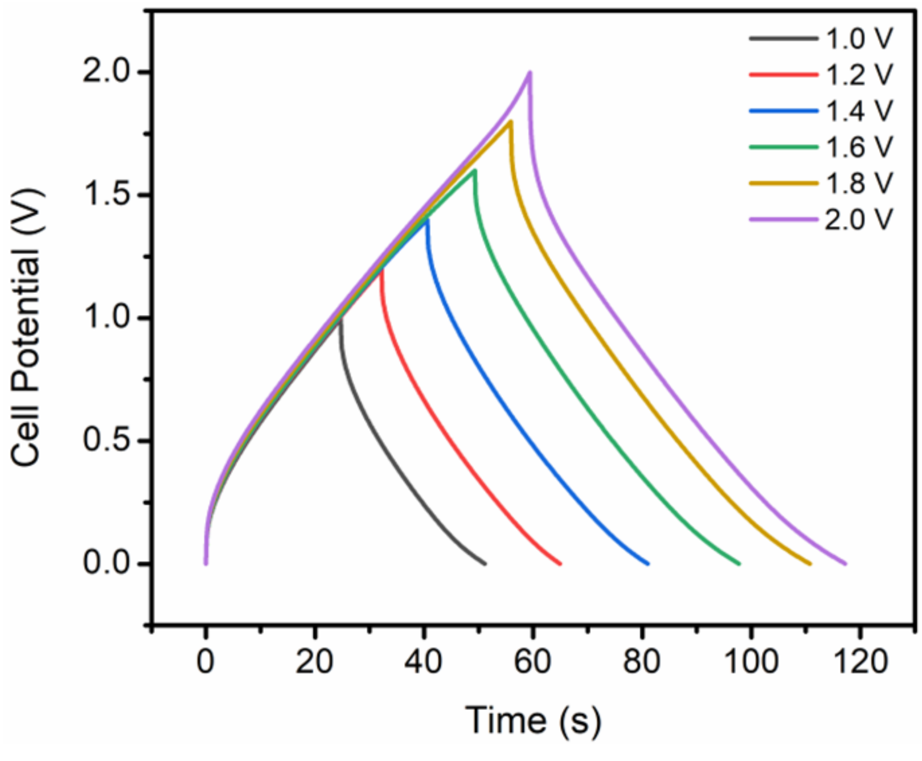

Fig. S22 GCD curves of N-doped V_4C_3/C//VO_2/VSe_2 ASC within different voltage windows ranging from 1 V to 2 V at 1 A/g current density.

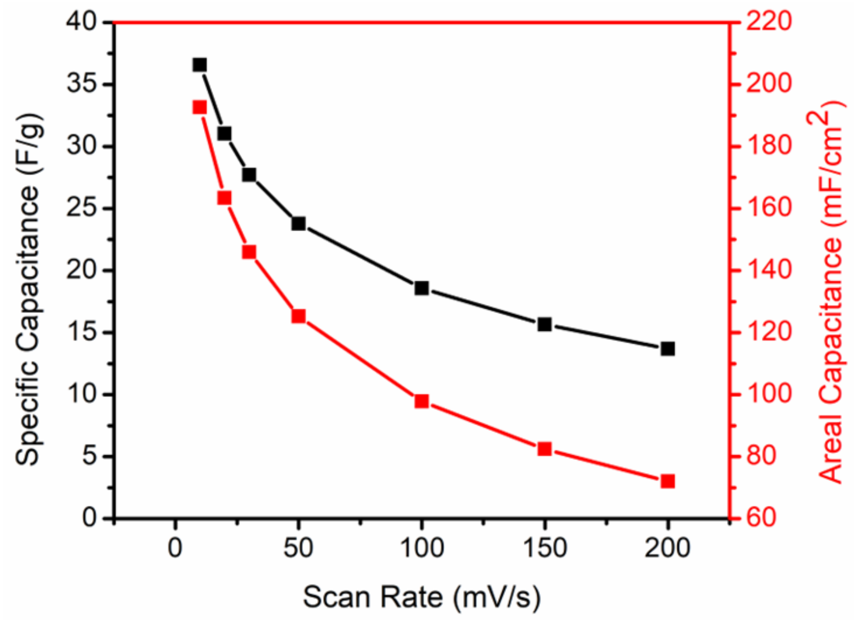

Fig. S23 Variation of capacitance values with scan rate for N-doped V_4C_3/C//VO_2/VSe_2 ASC.

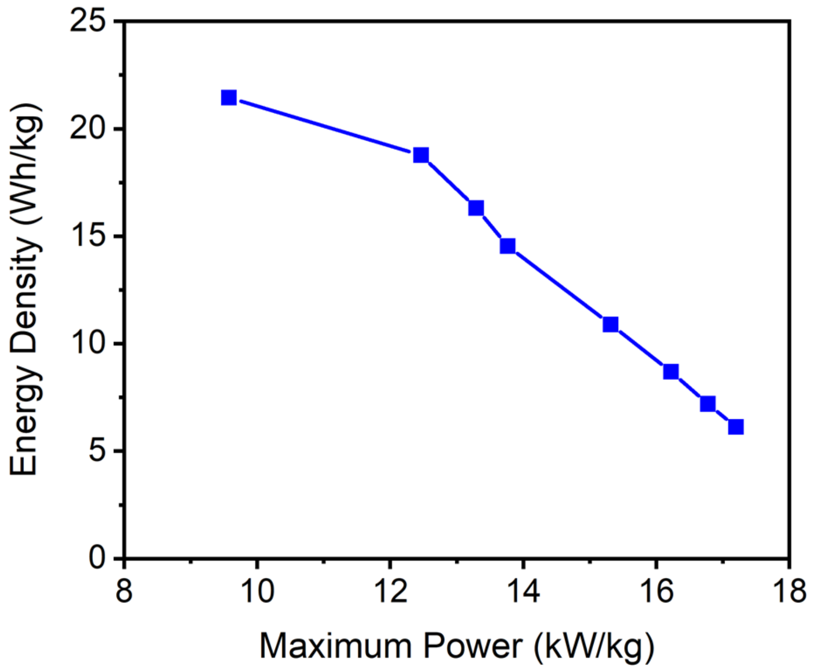

Fig. S24 The Ragone plot where the power densities are calculated using maximum power transfer theorem (Eq. 8).

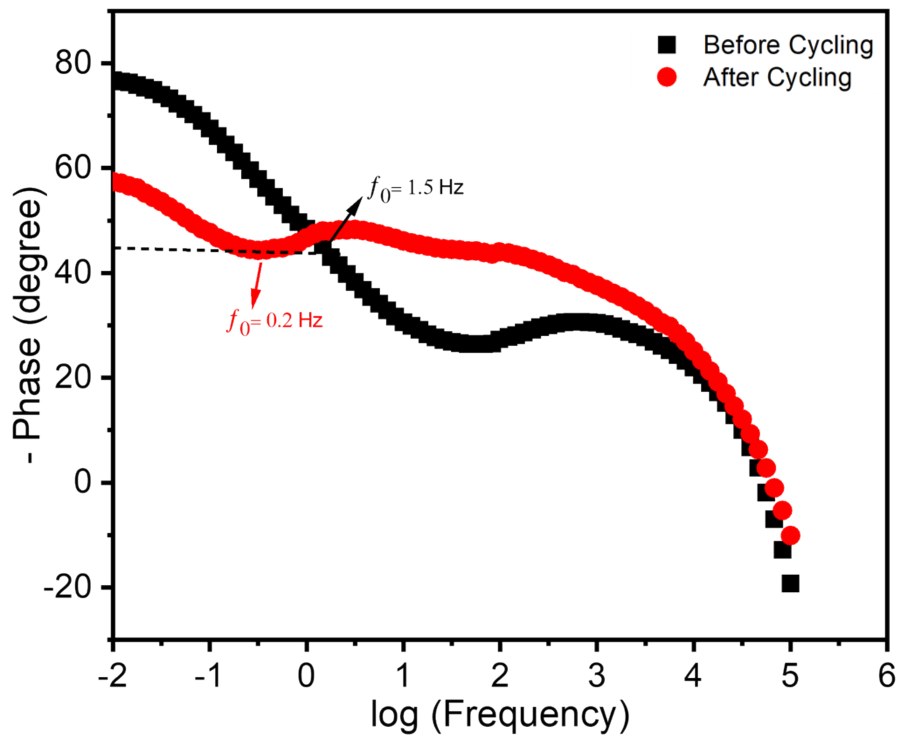

Fig. S25 The Bode plot of N-doped V_4C_3/C//VO_2/VSe_2 ASC before and after cycling test.

Table S1 Resistance values obtained before and after cycling tests by fitting Nyquist plots of single electrode as well as assembled ASC with equivalent circuit model as shown in the inset of Fig. 3i, Fig. 5f, and inset of Fig. 6i.

Type	Ohmic resistance (R_{el}, Ω)	Charge transfer resistance (R_{ct}, Ω)	Warburg impedance (R_w, Ω)
N-doped V_4C_3/C (before cycling)	1.4	0.5	-
N-doped V_4C_3/C (after cycling)	1.4	1.6	-
VO_2/VSe_2 (before cycling)	1.8	1.7	4
VO_2/VSe_2 (after cycling)	1.8	4.8	0.2
N-doped V_4C_3/C//VO_2/VSe_2 ASC (before cycling)	1.2	6.6	28.8
N-doped V_4C_3/C//VO_2/VSe_2 ASC (after cycling)	1	3000	62

Table S2 Comparison of electrochemical performance of N-doped V_4C_3/C and VO_2/VSe_2 with other pseudocapacitive materials.

Sl. No.	Material Used	Half-Cell Measurements			Full-Cell Measurements					Ref.
		Electrolyte	Specific Capacitance	Cyclic Retention	Full-Cell (+)//(-)	Electrolyte	Specific Capacitance	Max. Energy Density & Power Density	Cyclic Retention	
1	**N-doped V_4C_3/C**	**1M Na_2SO_4**	**118 F/g at 0.75 A/g**	**74% after 10000 cycles**	**N-doped V_4C_3/C// VO_2/VSe_2 ASC**	**1M Na_2SO_4**	**50.6 F/g at 0.25 A/g**	**21.4 Wh/kg and 4.5 kW/kg**	**78% after 5000 cycles**	**This Work**
2	**VO_2/VSe_2**	**1M Na_2SO_4**	**108.9 F/g at 0.25 A/g**	**97% after 10000 cycles**						
3	VN/V_2O_3/C	1M Na_2SO_4	112 F/g at 10 mV/s	99.4% after 4000 cycles	VN/V_2O_3/C SSC	1M Na_2SO_4	10.5 F/g at 10 mV/s	1.55 Wh/kg at 14 W/kg	87% after 2000 cycles	1
4	V_8C_7	1M Na_2SO_4	161.7 F/g at 1 A/g	92.8% after 10000 cycles	V_8C_7// AC ASC	1M Na_2SO_4	37.5 F/g at 1 A/g	16.9 Wh/kg at 8.7 kW/kg	100% after 5000 cycles	2
5	V_2NT_x Mxene (T_x = −F, −O)	3.5M KOH	112.8 F/g at 1.85 mA/cm^2	-	Mn_3O_4 //V_2NT_x MXene	3.5M KOH	25.3 F/g at 1.85 mA/cm^2	15.7 Wh/kg at 3748.4 W/kg	96% after 10000 cycles	3
6	VC	1M H_2SO_4	95.6 F/g at 1 A/g	38.9% after 10000 cycles	-	-	-	-	-	4
7	V_2O_3	1M $NaNO_3$	119 F/g at 0.05 A/g	-	-	-	-	-	-	5
8	V_2O_3/C	1M Na_2SO_4	146 F/g at 1 A/g	39.7% after 100 cycles	-	-	-	20.2 Wh/kg at 500 W/kg	-	6
9	VN	2M KOH	50.2 F/g at 1 A/g	-	-	-	-	-	-	7
10	VNNP@GO	2M KOH	109.7 F/g at 1 A/g	93% after 5000 cycles	-	-	-	-	-	7
11	$MoSe_2$	2M KOH	115 F/g at 2 A/g	64% after 2000 cycles	$MoSe_2$ SSC	2M KOH	4.1 F/g at 0.5 A/g	184.5 mWh/kg at 74.6 mW/kg	105% after 10000 cycles	8
12	MnSe(20)/Ni Co_2O_4	3M KOH	450.8 F/g at 0.1 A/g	-	MnSe(20)/Ni Co_2O_4// dip coated graphene	3M KOH	45.8 F/g at 0.1 A/g	12.4 Wh/kg at 70.0 W/kg	86% after 5000 cycles	9

13	$CoSe_2$	6M KOH	333.0 F/g at 1 A/g	-	$CoSe_2$//AC	6M KOH	56.7 F/g at 0.5 A/g	18.9 Wh/kg at 387 W/kg	100.9% after 25000 cycles	10
14	VOCNT@$Co_{0.85}$Se/NF	2M KOH	638 F/g at 1 A/g	97.3% after 5000 cycles	VOCNT@$Co_{0.85}$Se/NF//AC	2M KOH	91.5 F/g at 0.5 A/g	21.47 Wh/kg at 325 W/kg	112.7% after 3000 cycles	11
15	$NiSe_2$	1M KOH	75 F/g at 2 mV/s	92% after 5000 cycles	-	-	-	-	-	12
16	$Ni_{0.85}$Se-2	2M KOH	1010 F/g at 1 A/g	91.3% after 1000 cycles	$Ni_{0.85}$Se-2//AC ASC	2M KOH	45 F/g at 1 A/g	18.1 Wh/kg at 844.5 W/kg	82.2% after 3000 cycles	13
17	Zn-Co-Se	1M KOH	522.41 F/g at 0.5 A/g	93% after 3000 cycles	Zn-Co-Se//Graphene ink ASC	1M KOH	15.09 F/g at 0.2 A/g	16.97 Wh/kg at 539.63 W/kg	95% after 5000 cycles	14

References:

1. Y. Zhang, X. Wang, J. Zheng, T. Hu, X. Liu and C. Meng, *Appl. Surf. Sci.*, 2019, **471**, 842-851.
2. L. Zhang, W.-B. Zhang, Q. Zhang, X. Bao and X.-J. Ma, *Intermetallics*, 2020, **127**, 106976.
3. S. Venkateshalu, J. Cherusseri, M. Karnan, K.S. Kumar, P. Kollu, M. Sathish, J. Thomas, S.K. Jeong and A.N. Grace, *ACS Omega*, 2020, **5**, 17983-17992.
4. J. Gao, C. Xu, X. Tian, M. Sun, J. Zhao, J.-Y. Ma, H. Zhou, J. Xiao and M. Wu, *Sol. Energy*, 2020, **206**, 848-854.
5. X. Zhang, Z. Bu, R. Xu, B. Xie and H.-Y. Li, *Funct. Mater. Lett.*, 2017, **10**, 1750077.
6. J. Zheng, Y. Zhang, X. Jing, X. Liu, T. Hu, T. Lv, S. Zhang and C. Meng, *Colloids Surf. A: Physicochem. Eng. Asp.*, 2017, **518**, 188-196.
7. T. He, Z. Wang, X. Li, Y. Tan, Y. Liu, L. Kong, L. Kang, C. Chen and F. Ran, *J. Alloys Compd.*, 2019, **781**, 1054-1058.
8. S. Upadhyay and O.P. Pandey, *J. Alloys Compd.*, 2021, **857**, 157522.
9. V. Raman, D. Chinnadurai, R. Rajmohan, V.T. Chebrolu, V. Rajangam and H.-J. Kim, *New J. Chem.*, 2019, **43**, 12630-12640.
10. S. Liu, S. Sarwar, J. Wang, H. Zhang, T. Li, J. Luo and X. Zhang, *J. Mater. Chem. C*, 2021, **9**, 228-237.
11. H. Chen, W. Li, M. He, X. Chang, X. Zheng and Z. Ren, *J. Alloys Compd.*, 2021, **855**, 157506.
12. N.S. Arul and J.I. Han, *Mater. Lett.*, 2016, **181**, 345-349.
13. Q. Yang, X. Chen, H. Zhan, S. Wu, Q. Hu, R. Zhou and Y. Xue, *Synth. Met.*, 2019, **257**, 116167.
14. V.T. Chebrolu, B. Balakrishnan, D. Chinnadurai and H.J. Kim, *Adv. Mater. Technol.*, 2020, **5**, 1900873.